한국측량학회지, 제 25권 제 6-1호, pp. 517~528(2007년 12월 31일)

# Implementation of Digital Image Processing for Coastline Extraction from Synthetic Aperture Radar Imagery

Dong-Cheon Lee[1] · Suyoung Seo[2] · Impyeong Lee[3] · Jay Hyoun Kwon[4] · Grady H. Tuell[5]

**Abstract**

Extraction of the coastal boundary is important because the boundary serves as a reference in the demarcation of maritime zones such as territorial sea, contiguous zone, and exclusive economic zone. Accurate nautical charts also depend on well established, accurate, consistent, and current coastline delineation. However, to identify the precise location of the coastal boundary is a difficult task due to tidal and wave motions. This paper presents an efficient way to extract coastlines by applying digital image processing techniques to Synthetic Aperture Radar (SAR) imagery. Over the past few years, satellite-based SAR and high resolution airborne SAR images have become available, and SAR has been evaluated as a new mapping technology. Using remotely sensed data gives benefits in several aspects, especially SAR is largely unaffected by weather constraints, is operational at night time over a large area, and provides high contrast between water and land areas. Various image processing techniques including region growing, texture-based image segmentation, local entropy method, and refinement with image pyramid were implemented to extract the coastline in this study. Finally, the results were compared with existing coastline data derived from aerial photographs.

Keywords : SAR image, Coastline, Digital image processing, Accuracy assessment

## 1. Introduction

Coastlines provide important baseline data for demarcating marine territorial limits that might be crucial information to resolve territory disputes, and for geographic referencing needed to manage coastal resources. Moreover, accurately extracted coastline information can be widely used in a Geographic Information System (GIS). The most efficient data to identify land-water interfaces and to monitor a coastline over large areas is images, among which aerial photographs have been the primary data source for mean high water (MHW) and mean lower low water (MLLW) mensuration. However, weather condition is one of the serious limiting factors in the acquisition of optical imagery. Often, images for coastline extraction are not available at the appropriate tidal stage with a sun angle acceptable for correct exposure of the film in a timely manner.

SAR imagery has proven its potential to meet the demanding application of precise coastline mapping to overcome the disadvantages of using optical images. For instance, the Remote Sensing Division of the National Geodetic Survey (NGS) at the National Oceanic and Atmospheric Administration (NOAA) has been utilizing state-of-the-art techniques including SAR for accurate and efficient coastal mapping for improvement and revision of navigation charts, for accurate storm surge modeling, coastal flooding, and pollution trajectory modeling, for establishment of land and marine GIS, and for environmental analysis and monitoring (Tuell, 1998; NOAA's Coastal Mapping Web-site, 2004).

Airborne SAR and Radarsat SAR images were used in this study to detect the land-water boundary with different image processing methods. One of the recent

1) Corresponding Author · Department of Geoinformation Engineering, Sejong University (E-mail: dclee@sejong.ac.kr)
2) Inha University (Email: Suyoung.Seo@gmail.com)
3) Department of Geoinformatics, The University of Seoul (E-mail: iplee@uos.ac.kr)
4) Department of Geoinformatics, The University of Seoul (E-mail: jkwon@uos.ac.kr)
5) Optech International (E-mail: grady@optech.on.ca)

relevant works could be found in Lue and Kenneth (2004). They utilized Radarsat imagery and histogram-based statistical image processing to extract the coastline of Antarctica. Image processing is the key technique in the extraction of coastlines. The major objectives of digital image processing are manipulation and interpretation of the scene data to improve pictorial quality and to extract information. The important issue in image processing is to choose an appropriate image processing method. It is not easy, however, because the image processing task is inherently dependent upon the image quality and contents, level of detail, and purpose. Moreover, a unique method or optimal scheme is not always available in many cases. Often an ad hoc image processing scheme is applied to the specific purpose such as coastal boundary extraction. However, best results may not be guaranteed with such a scheme.

In this study, various digital image processing schemes such as region growing, texture-based image segmentation, entropy method, and refinement strategy of the extracted coastline were employed to demonstrate the feasibility of using SAR imagery for extracting the coastline. It is well known that the most promising method in any image processing is to resemble the human vision system that utilizes all possible visual cues. In that sense, an adaptive texture-based feature analysis strategy was included in the processing schemes (Lee and Schenk, 1998). In order to evaluate the results, the extracted coastal boundary was registered to existing coastline map generated by aerial photogrammetry. However, because of the small scale of the map and unavailability of ground truth such as in-situ surveying data and topographic information, only limited analysis of the results was possible.

## 2. Study Site and Test Data

The study site is located on the north coast of Castle Bay, Alaska (Fig. 1). Fig. 2 shows an 8-m resolution Radarsat SAR image and a 1-m resolution airborne SAR image acquired in 1997 by the Environmental Research Institute of Michigan (ERIM) used to implement coastline extraction. As a strategy to mitigate the layover effect, the flight lines for coastal mapping were designed with a flying height of 4,200 m with a depression angle of 30°. The airborne SAR image covers the area 158.1964°W - 158.2508°W, 56.2575°N - 56.2916°N. The radarsat image covers a portion of the airborne SAR image (Fig. 2 (b)).

## 3. Image Processing Schemes and Experimental Results

Extraction of the coastline from Radarsat SAR was independently implemented by region growing, texture-based scheme, and entropy method. Then, the refinement of the coastline was carried out with high resolution airborne SAR imagery based on image pyramid approach.

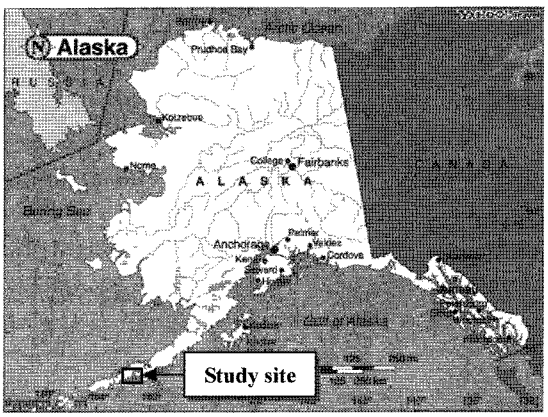


Fig. 1. Study site (Castle Bay, Alaska)

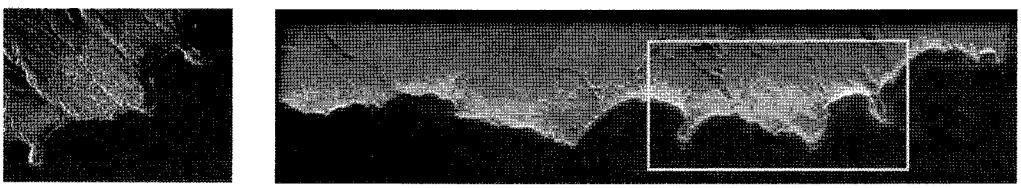

(a) Radarsat SAR image (b) Airborne SAR image (boxed area indicates Radarsat image coverage)

Fig. 2. Test images (Courtesy of Sandia National Labs)

### 3.1 Region Growing Method

Region growing is one of the region-based image segmentation methods. The basic concept of this method is that the neighboring pixels of similar property are grouped together to form a region (Pratt, 2001). The region growing process consists of initial segmentation and region merging. Selection of seed pixels and forming regions from the seed pixels are performed in the initial segmentation step. Regions with small area (*i.e.*, a few pixels) or regions surrounded completely by a larger region are merged into the larger region in the region merging step. Fig. 3 describes the procedure of region growing. The result of region growing is shown in Fig. 4.

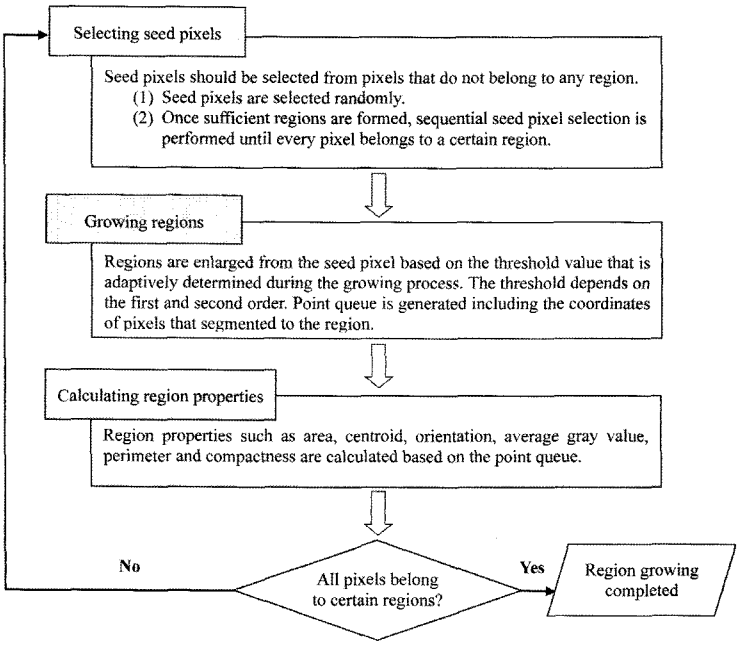


Fig. 3. Procedure of region growing

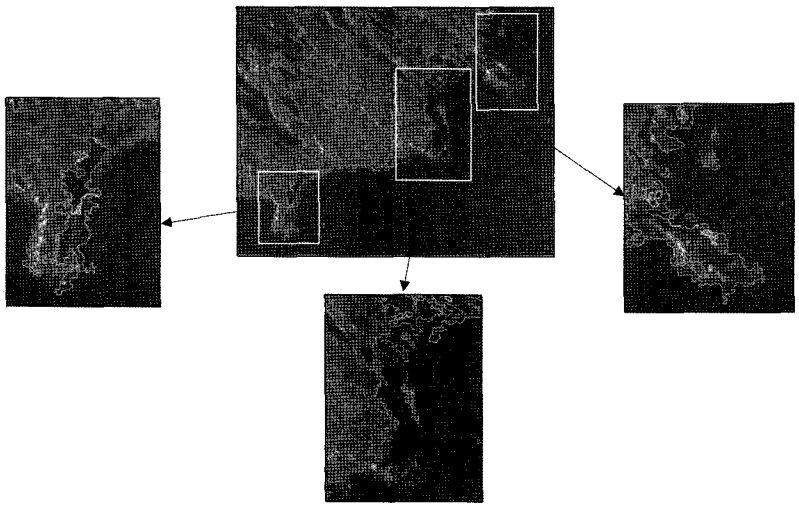

Fig. 4. Region growing applied to segmentation of Radarsat image

### 3.2 Adaptive Texture-based Method

SAR images include speckle noises that are signal dependent. In consequence, land and water areas might have different noise patterns that could be interpreted as different textures. Implementation of the adaptive approach of texture-based feature analysis with Gabor functions attempts to discriminate different texture patterns that lead to identification of the land-water interface. Two-dimensional Gabor functions were implemented for human visual information processing to segment the image. A Gabor function is defined by a harmonic oscillator which is a complex sinusoidal plane wave of some frequency and orientation within a Gaussian envelope (Daugman, 1985). The general form of two-dimensional Gabor functions is given by

$$G(x,y) = g(x,y)\cdot \exp[2\pi i(Ux+Vy)] \tag{1}$$

where $i=\sqrt{-1}$, $U=F\cos\theta$, $V=F\sin\theta$, $\theta$ represents orientation, $F=\frac{1}{T}$, and T is wavelength. g($x$, $y$) is a two-dimensional Gaussian function given by

$$g(x,y) = \frac{1}{2\pi\sigma_x\sigma_y}\exp\left[-\left(\frac{x^2}{2\sigma_x}+\frac{y^2}{2\sigma_y}\right)\right] \tag{2}$$

where $\sigma_x$ and $\sigma_y$ are the standard deviations with respect to the $x$-axis and $y$-axis. Therefore, two-dimensional Gabor functions with the unity aspect ratio of the Gaussian function can be expressed as

$$G(x,y) = \exp\left[-\frac{(x-x_o)^2+(y-y_o)^2}{2\sigma^2}\right] \cdot \sin\{\omega(x\cos\theta - y\sin\theta)+\varphi\} \tag{3}$$

where $x_o$ and $y_o$ specify the center of the Gaussian function, $\omega = 2\pi F$ is the angular frequency, and $\varphi$ is the phase shift. The two-dimensional Gabor functions have real and imaginary components. The phase shift generates real components for $\varphi = 90°$ and imaginary components for $\varphi = 0°$ (Bovik et al., 1990; Dunn and Higgins, 1995). The two-dimensional Gabor function is shown in Fig. 5.

There are four parameters in a two-dimensional Gabor function: the standard deviation of the Gaussian envelope ($\sigma$), spatial frequency ($\omega$), orientation ($\theta$), and phase ($\varphi$). These parameters characterize primitives of the images. The determination of the appropriate parameters is the most important task in utilizing Gabor filters to extract pictorial information. All possible combinations of the parameters result in a large set of filters. The properties of the parameters are described as follows:

(1) Standard deviation: The standard deviation of the Gaussian envelope controls the spatial extent as well as the band width of the filters. Physiological evidence suggests a tendency toward decreasing spatial extent with increasing frequency preference (Turner, 1986).

(2) Spatial frequency: The number of cycles per period determines the spatial frequency that is related to the size of the primitives. It controls the resolution that is related to the amount of information. Various resolutions are obtained as different generations of

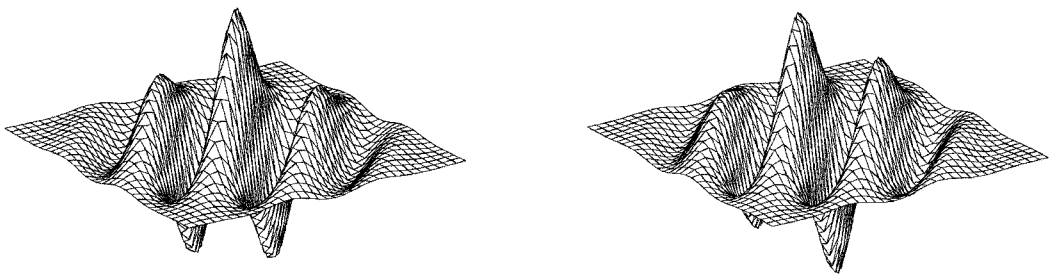

(a) Real component (b) Imaginary component

Fig. 5. Perspective view of 2D Gabor functions

wavelets are created by varying dilation factors.

(3) Orientation: Proper selection of the orientation can determine directionality or dominant orientation of the primitives. Orientation preference is a particularly important feature of simple cells in the visual cortex in the human vision system. Their maximum response occurs where edges are oriented at a particular angle to the visual axis.

(4) Phase: Two-dimensional Gabor functions are composed of real and imaginary components with a 90° phase shift between them. The phase can solve the ambiguity problem. However, it cannot be decided unequivocally which parameter variation is responsible for the activity of the filter change.

A texture-based image segmentation scheme is summarized in Fig. 6. The image is segmented and subdivided further in progressive fashion based on the statistical property. A texton image which contains primitives such as blobs is generated by applying a Laplacian-of-Gaussian (LoG) operator (Schenk, 1999). The role of the texton image is to provide information for determining optimal parameters of the Gabor functions. Adaptive processing of Gabor functions with the parameters is performed for a progressively subdivided region of the image. In this study, an iterative self organizing data analysis technique (ISODATA) clustering was employed

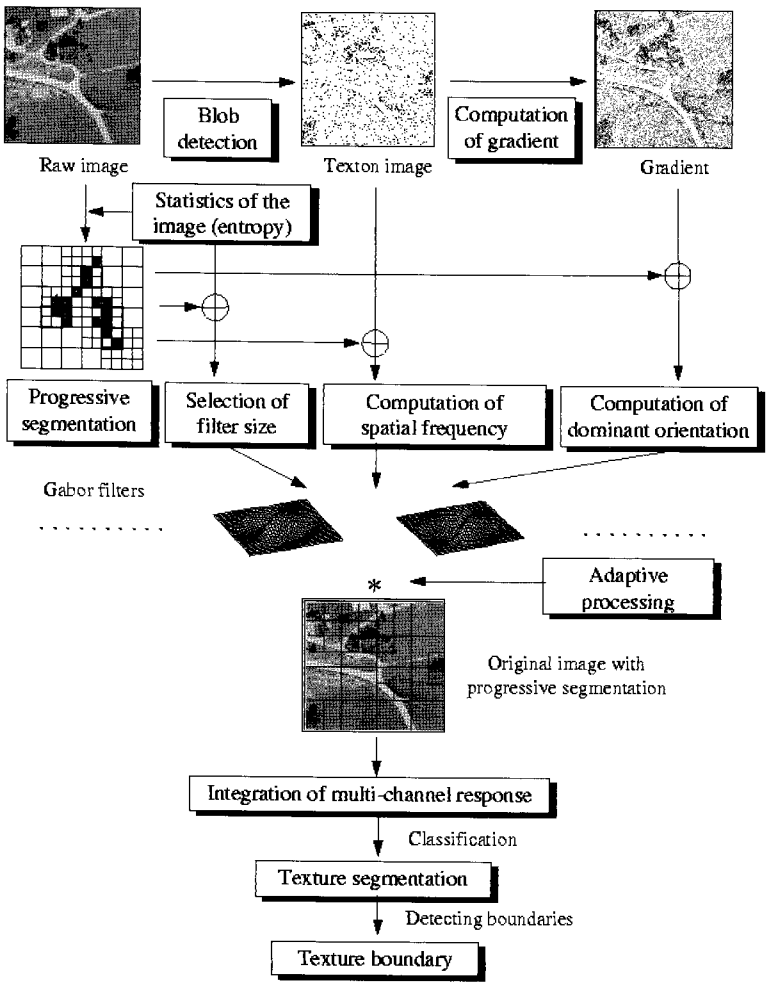


Fig. 6. Adaptive texture-based image segmentation scheme

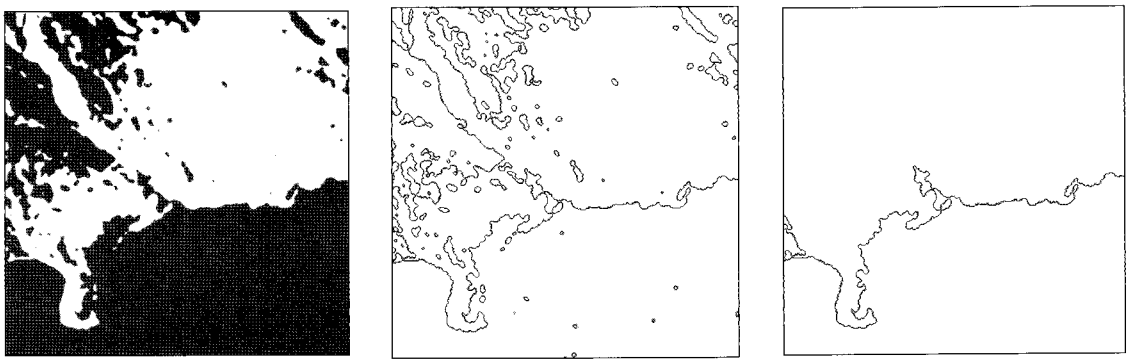

(a) Segmented image (b) Segmented boundary (c) Extracted coastline

Fig. 7. Adaptive texture-based segmentation and coastline extraction

to delineate the land-water boundary. The results from adaptive texture-based segmentation are displayed in Fig. 7.

### 3.3 Local Entropy Method

SAR imagery of the study site has two distinct regions of land and water. The feature characteristics of land and water are heterogeneous and homogeneous, respectively. In this case, one can use the entropy, which is a measure of the degree of randomness of the variables, to differentiate distinct areas. Modification of the conventional entropy is necessary to normalize local kernels and measure randomness of the images that will eventually be the basic criteria for segmenting land and water areas. The modified entropy is expressed by

$$H = -\frac{n}{\log_2(n/b)} \sum_{i=0}^{n} p(i) \log_2 p(i) \qquad (4)$$

where $n$ is number of variables, $p(i)$ is probability corresponding to $i$, $i$ is a certain gray value, and $b$ is bin size (Jähne and Hauβecker, 2000). A three-level image pyramid was generated by Gaussian operator, then the entropy of each level was computed with different kernel sizes, 5x5, 7x7, and 11x11. Fig. 8 shows the distribution of the original histogram to bi-modal distribution after applying the entropy kernel. Therefore, entropy measurement provides an efficient way to determine the threshold value for separating distinct regions. Fig. 9 represents coastlines extracted by the entropy method with different kernel size through the image pyramid.

Producing maps involves generalization that depends on the scale and purpose of the map. The coarse level (second level in Fig. 9) shows a smooth coastline that could not depict details and small features are merged.

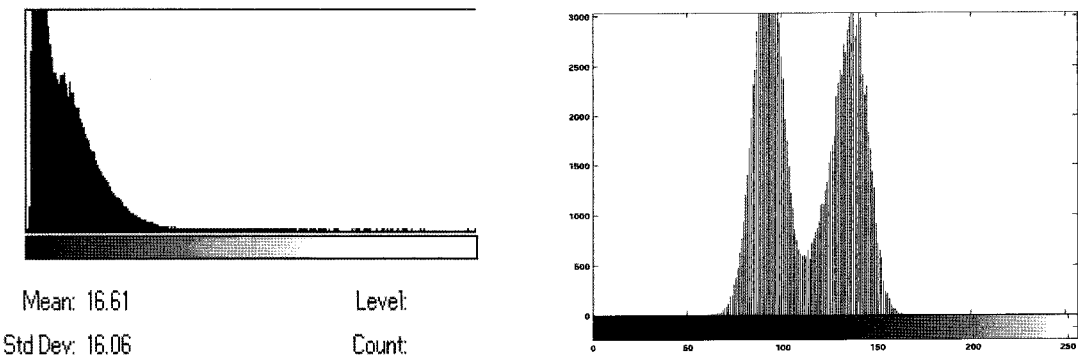


(a) Radarsat SAR image (b) Entropy image

Fig. 8. Example of histograms of the original and entropy images

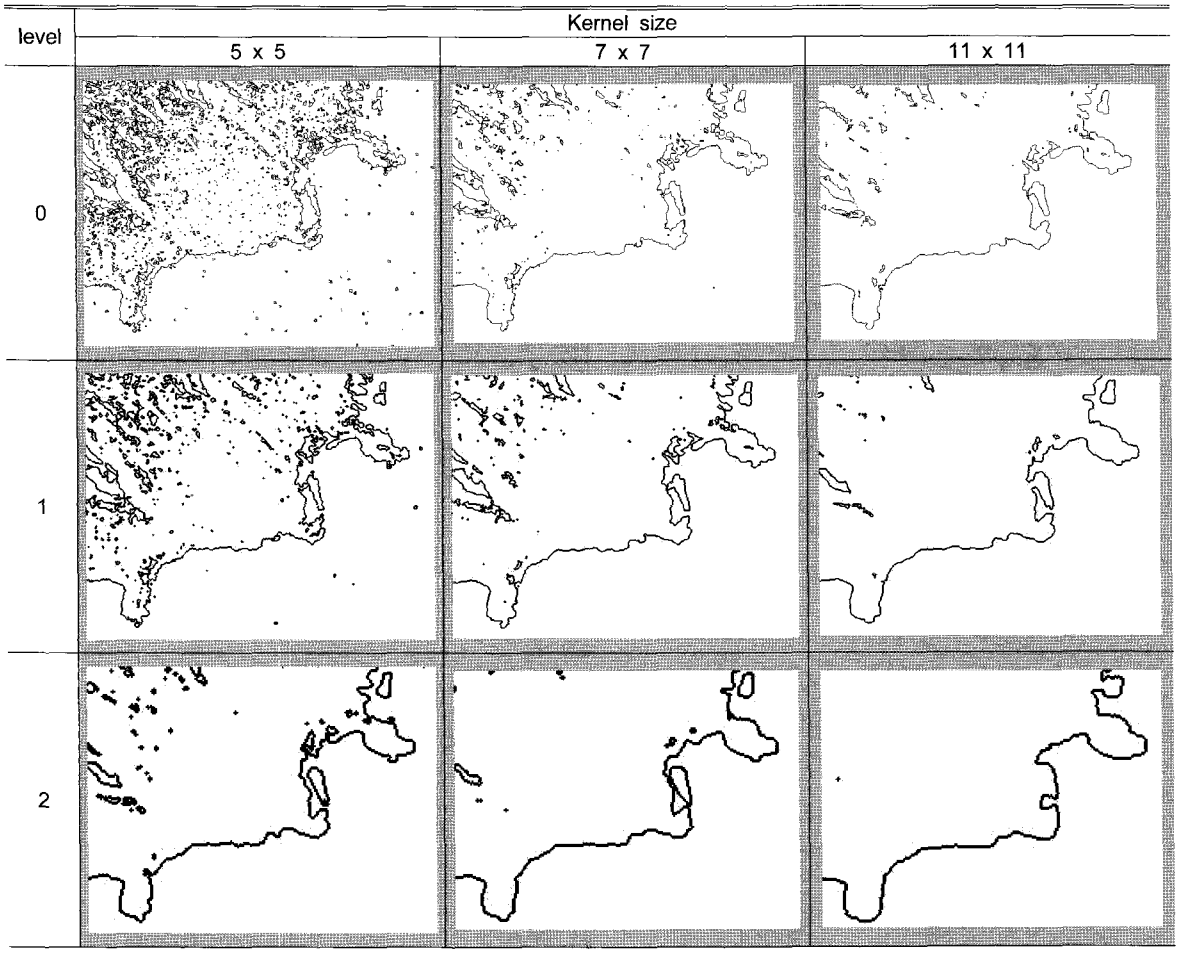


Fig. 9. Results from local entropy method

Therefore, the coarse level image is suitable for mapping small-scale coastlines.

### 3.4 Refinement Scheme with Image Pyramid

#### 3.4.1 Histogram Thresholding Method

One of the major benefits from the image pyramid approach is efficiency. In addition, speckle noise of SAR imagery can be reduced at the coarse level of the image pyramid. Approximate coastlines are extracted at the coarse level; then accurate ones are obtained at the fine level by utilizing information from the coarse level image. The initial coastline was extracted using a histogram threshold. The histogram of the coastal region in the coarse level has bi-modal distribution that represents land and water because most feature details are suppressed. The procedure of this method is summarized as follows:

(1) Extract land-water boundary between segmented regions.
(2) Select a pixel on the boundary extracted from the coarse level.
(3) Define a local window centered on the selected point in the fine level.
(4) Extract the boundary in the local window using the same procedure applied for the coarse level.

Fig. 10 shows initial coastline at the coarse level of the airborne SAR image.

Fig. 11 shows refinement steps for a selected area. The selected area especially has a complex shape and the presence of radar shadow. Fig. 12 shows result of the initial and refined coastlines.

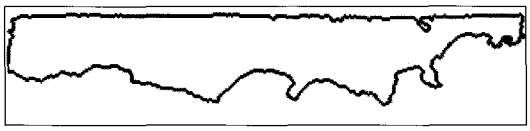

(a) Extracted coastline at coarse level

(b) Superimposed coastline on the image

Fig. 10. Initial coastline extracted at the coarse level

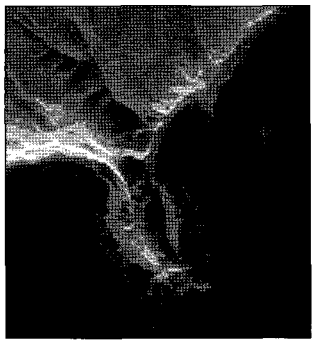

(a) Selected local window

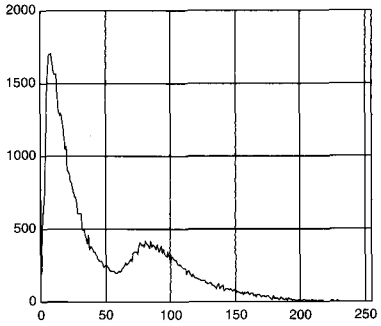


(b) Histogram of local window

(c) Segmentation using histogram thresholding

(d) Merging of segmented image

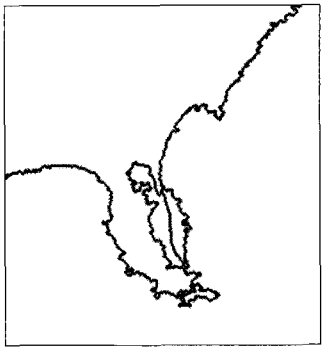

(e) Extracted boundary

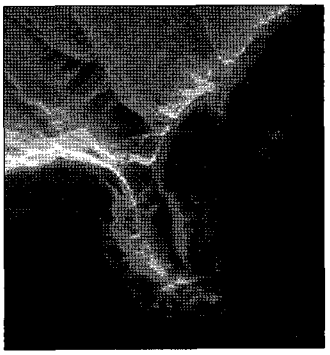

(f) Coastline superimposed on the image

Fig. 11. Extraction of coastline from the local window on the fine level

3.4.2 Gradient Method

Another refinement strategy to produce an accurate coastline is to utilize the initial coastline derived from the coarse level of the image, then search for a pixel having significant gradient from the initial coastline (Fig. 13 (a)). The search was performed for eight directions (Fig. 13 (b)). Once the pixel was found the coastline detection starts from the pixel by computing the gradient of the gray values pixel-by-pixel for eight directions. Fig. 14 shows the experimental result of the refinement.

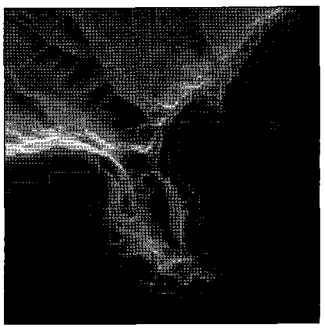

Fig. 12. Superimposition of initial coastline and refined coastline (Red line: Initial coastline, blue line: Refined coastline)

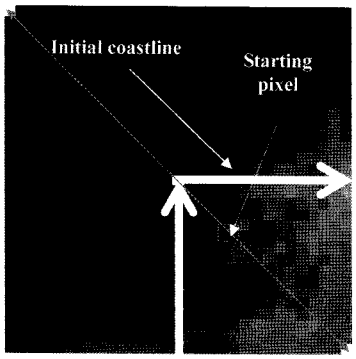


(a) Initial coastline and searching for starting pixel

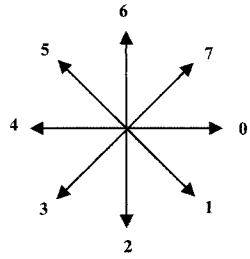


(b) Search directions

Fig. 13. Refinement scheme based on gradient using initial coastline

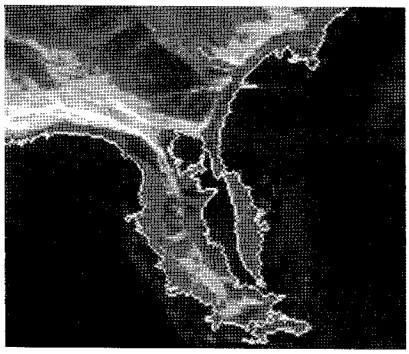

Fig. 14. Refined coastline by gradient method.

## 4. Analysis and Evaluation

### 4.1 Comparison of Methods

A large variety of digital image processing methods have been developed and the image segmentation methods can be categorized into edge-based and region-based approach (Schalkoff, 1989). Also other categorization of the methods is available such as image-domain and frequency-domain approach. The implemented digital image processing methods are region-based approach and these methods are more meaningful and appropriate for segmenting land and water regions with SAR images than pixel-based or edge-based approaches which consider simply gray-value variations. Especially, SAR image data provides rich textural information and terrain surface characteristics than optical imagery.

Even though many different image processing techniques are available, it is not easy to select optimal one because each method has inherent shortcomings and processing results largely depend on the image quality, contents, sensor type, and other external conditions including data acquisition mechanism, characteristics of the surface, image scale and so on. Table 1 describes summary of the properties of each method based on the experiments.

### 4.2 Accuracy Evaluation

In general, assessing the accuracy of a SAR-derived coastline is difficult because of significant time difference from the reference map and uncertainty of the tidal stage. Therefore, instead of evaluating the accuracy of each individual result from this study, the overall methodology of accuracy evaluation is discussed. The evaluation is based on a comparison between the SAR-derived coastline and a photogrammetrically-derived coastline after image-to-map registration. Affine transformation was employed for the registration. Affine transformation models geometric distortions in remote sensing imagery including shifts, scale changes, orthogonality, and rotation between the coordinate systems (Jensen, 1996; Schowengertdt, 1997). The affine transformation between the map and SAR image is expressed as

$$X_{SAR} = a_{11}X_{MAP} + a_{12}Y_{MAP} + a_{13} \quad (5\text{-}1)$$

$$Y_{SAR} = a_{21}X_{MAP} + a_{22}Y_{MAP} + a_{23} \quad (5\text{-}2)$$

where $X_{SAR}$ and $Y_{SAR}$ are coordinates of the SAR-derived coastline, while $X_{MAP}$ and $Y_{MAP}$ are corresponding coordinates in the map complied from aerial photographs, and $a_{11}$, ···, $a_{23}$ are the transformation parameters.

Table 1. Comparison of image processing methods

| Methods | | Advantage | Disadvantage | Comment | |
|---|---|---|---|---|---|
| Segmentation and coastal line extraction | Region growing | • Conceptually simple approach<br>• Effective for images with a few regions | • Depends on seed pixels<br>• Suffer from conflicting problem | SAR imagery of coastal areas has a few regions. Therefore, reasonable result to segment land/homogeneous water interface was obtained. | |
| | Adaptive texture-based | • Textural information extracted<br>• Segmentation with meaningful regions | • Conceptually and computationally complicated<br>• Requires adaptive strategy<br>• Difficult algorithm to implement | Globally meaningful segmentation can be obtained. However, refinement procedure is required for extracting detail coastline. | |
| | Local Entropy | • Simple computation<br>• Easy to implement<br>• Appropriate to segment distinct binary regions | • Depends on thresholding value<br>• Requires modification for local areas | Two distinct regions can be reasonably separated. Therefore, extraction results of the land-water interface are acceptable. | |
| Refinement with image pyramid | Histogram threshold | • Less sensitive to noise<br>• Simple method | • Depends on thresholding value<br>• Detect global features | Image pyramid is useful for efficient refinement of the coastline. | Coastline is efficiently extracted. It is suitable for small scale coastline mapping. |
| | Gradient | • Detect local detail features<br>• Extract accurate boundary | • Sensitive to noise<br>• Extract unnecessarily detail coastline | | Accurate coastline is extracted. Therefore, it is recommendable for large scale coastline mapping. |

An accuracy assessment of the SAR-derived coastline was performed by computing the root mean square error (RMSE) of the planimetric errors. The planimetric error, $e$, for each control point and checkpoint is computed by

$$e = \sqrt{(X'_{SAR} - X_{MAP})^2 + (Y'_{SAR} - Y_{MAP})^2} \quad (6)$$

where $X'_{SAR}$ and $Y'_{SAR}$ are coordinates of the SAR-derived coastline after registration. The RMSE of the planimetric error is computed by

$$RMSE = \sqrt{\frac{\sum_{i=1}^{n} e^2}{n}} \quad (7)$$

where $n$ is number of points (Maling, 1989).

The RMSE represents the relative accuracy of the Radarsat SAR-derived coastline. Evaluation was not performed for an airborne SAR-derived coastline because the reference data is a small scale map that could not represent details and fine features. Traditionally, mapping for coastal areas has been carried out by compiling aerial photographs. The study area had been previously mapped by the National Geodetic Survey at NOAA using aerial photogrammetry in 1991 (Fig. 16 (a)) that serves as the primary data set for the evaluation of the SAR-derived coastline (Tuell, 1998). Since the base map for accuracy evaluation is a small scale, result from the entropy method with 7x7 kernel size was evaluated here. Based on the visual inspection and preliminary tests, the extracted coastline was interpreted as corresponding to MLLW from an aerial photograph compiled map. Seven control points were selected to determine the transformation parameters through the least-squares method, then the RMSE of the control points and check points were computed.

Fig. 15 shows the distribution of control and check points on the extracted coastlines from aerial photographs and the SAR image. Fig. 16 shows superposition of the coastlines after registration using affine transformation. The evaluation result is summarized in Table 2. The accuracy in this experiment is not absolute because actual reference data are not available, but a scanned map published in Tuell (1998) was used. Once vector data of the coastline or ground surveying data that could serve as reference are available, absolute accuracy can be

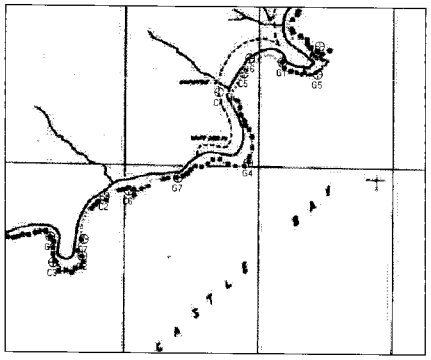

(a) Map compiled with aerial photographs (Solid line and dotted line in the map represent MHW and MLLW, respectively.)

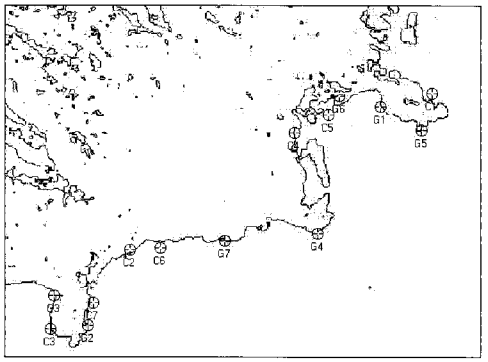

(b) Coastline extracted from radar SAR image (G1-G7: Control points, C1-C2: Check points)

Fig. 15. Distribution of control and check points on the extracted coastlines.

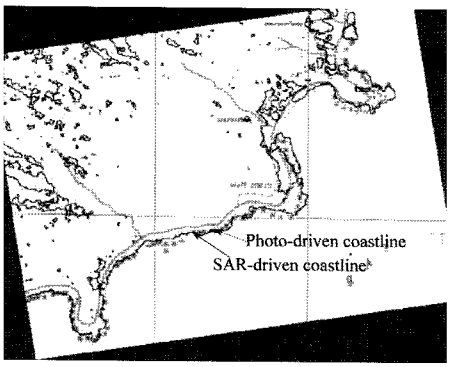


Fig. 16. Superimposition of the coastlines after registration using affine transformation

performed using the method described above.

## 5. Concluding Remarks

Imagery acquired by optical sensors and photogrammetrically compiled images have been primary data sources for mapping coastal areas in past years. The procedure using optical imagery is well established and provides accurate results. However, often weather condition is a limiting factor in the acquisition of optical imagery. In general, images for coastline extraction are not available at the appropriate tidal stage with a sun

Table 2. Accuracy of Radarsat image derived coastline (unit: pixel)

| Type | ID | SAR image | | Map | | Residuals after transformation | | Planimetric error | RMSE |
|---|---|---|---|---|---|---|---|---|---|
| | | X | Y | X | Y | X | Y | | |
| Control | G1 | 442.81 | -121.05 | 429.00 | -413.00 | -0.37 | -0.68 | 0.77 | 1.05 |
| | G2 | 99.11 | -376.52 | 207.37 | -627.87 | 1.37 | -0.93 | 1.66 | |
| | G3 | 59.11 | -341.77 | 171.67 | -606.85 | -1.30 | 0.85 | 1.55 | |
| | G4 | 369.15 | -269.13 | 391.79 | -523.87 | -0.33 | -0.13 | 0.35 | |
| | G5 | 491.63 | -148.43 | 467.81 | -425.90 | -0.25 | 0.85 | 0.89 | |
| | G6 | 394.41 | -108.06 | 392.87 | -408.62 | 0.88 | -0.25 | 0.91 | |
| | G7 | 260.07 | -277.58 | 313.00 | -541.00 | 0.00 | 0.29 | 0.29 | |
| Check | C1 | 504.27 | -105.27 | 470.56 | -395.02 | -2.57 | 0.28 | 2.58 | 1.92 |
| | C2 | 148.43 | -288.45 | 231.56 | -561.94 | -1.35 | -1.68 | 2.15 | |
| | C3 | 54.22 | -381.49 | 175.00 | -635.00 | 1.60 | 0.61 | 1.71 | |
| | C4 | 342.14 | -151.59 | 358.74 | -446.22 | -0.49 | -2.41 | 2.46 | |
| | C5 | 382.30 | -130.43 | 387.00 | -425.00 | 1.60 | 0.40 | 1.65 | |
| | C6 | 184.45 | -286.74 | 259.00 | -555.00 | 0.66 | 0.77 | 1.02 | |
| | C7 | 105.77 | -350.60 | 209.00 | -609.00 | 0.99 | -0.78 | 1.26 | |

angle acceptable for correct exposure of the film in a timely manner. However, SAR is largely unaffected by the presence of cloud cover, and it delivers flexibility over weather conditions. In addition, SAR produces a distinct land-water interface because the SAR signal is absorbed in water. Various image processing techniques were implemented to extract the coastline from SAR imagery automatically. Based on the experiments, the following conclusions and future recommendation are drawn:

1. SAR imagery has the potential to meet the demanding purpose of coastline extraction.
2. The resulting coastline depends on the resolution of the imagery as well as the image processing methods implemented.
3. Base upon the experiments, local entropy method provided acceptable result because this method is appropriate for segmenting two distinct regions such as land and water areas.
4. Refinement is recommended to produce an accurate coastline. Especially the image pyramid approach is efficient for the refinement process. Thresholding and gradient method are suitable for small-scale and large-scale coastline mapping purposes, respectively.
5. Geo-referencing of the SAR imagery with reference data at the same tidal stage is required for assessment of absolute accuracy.
6. For the future study, topographic information such as a Digital Elevation Model (DEM) over the coastal area including the sea floor can be acquired by utilizing LiDAR (Light Detection And Ranging). Such additional data with appropriate information fusion would be most useful in extraction of the accurate land-water boundary.

## Acknowledgements

This study was supported by NGS (National Geodetic Survey) / NOAA (National Oceanic & Atmospheric Administration). Authors would like to thank Ms. Irene Tesfai at The Ohio State University for her help with this manuscript.

## References

Bovik, A., Clark, M. and Geisler, W. (1990), Multichannel Texture Analysis Using Localized Spatial Filters. *IEEE Transactions on Pattern Analysis and Machine Intelligence*, 12, pp. 55-73.

Daugman, J. (1985), Uncertainty Relation for resolution in Space, Spatial Frequency, and Orientation Optimized by Two-Dimensional Visual Cortical Filters. *Journal of Optical Society of America*, 7, pp. 1160-1169.

Dunn, D. and Higgins, W. (1995), Optimal Gabor Filters for Texture Segmentation. *IEEE Transactions on Image Processing*, 4, pp. 947-964.

Jähne, B. and Hauβecker, H. (2000), *Computer Vision and Applications*. Academic Press, San Diego, 679 p.

Jensen, J. (1996), *Introductory Digital Image Processing: A Remote Sensing Perspective*, 2nd ed. Prentice-Hall, Inc., Upper Saddle River, 318 p.

Lee, D.C. and Schenk, T. (1998), An Adaptive Approach for Extracting Texture Information and Segmentation. *International Archives of Photogrammetry and Remote Sensing*, 32-3/1, pp. 250-255.

Lui, H. and Kenneth, J. (2004), A Complete High-Resolution Coastline of Antarctica Extracted from Orthorectified Radarsat SAR Imagery. *Photogrammetric Engineering & Remote Sensing*, 70, pp. 605-615.

Maling, D. (1989), Measurements from Maps: Principles and Methods of Cartometry, Pergamon Press, Oxford, 577 p.

NOAA's Coastal Mapping Web-site, http://www.ngs.noaa.gov/RSD/coastal/index.html.

Pratt, W. (2001), *Digital Image Processing*, 3rd ed. John Wiley & Sons, Inc., New York, 735 p.

Russ, J. (2002), *The Image Processing Handbook*, 4th ed. CRC Press, Raleigh, 732 p.

Schalkoff, R. (1989), *Digital Image Processing and Computer Vision*, John Wiley & Sons, New York, 489 p.

Schenk, T. (1999), *Digital Photogrammetry*, Vol. 1, Terra-Science, Laurelville, 428p.

Schowengertdt, R. (1997), *Remote Sensing: Models and Methods for Image Processing*, 2nd ed. Academic Press, San Diego, 522p.

Tuell, G. (1998), The Use of High Resolution Airborne Synthetic Aperture Radar (SAR) for Shoreline Mapping. *International Archives of Photogrammetry & Remote Sensing*, 32-3/2, pp. 592-611.

Turner, M. (1986), *Texture Discrimination by Gabor Function*, Biological Cybernetics, 55, pp. 71-82.

(접수일 2007. 10. 10, 심사일 2007. 11. 20, 심사완료일 2007. 12. 17)